Nano Energy 108 (2023) 108237

Contents lists available at ScienceDirect

Nano Energy

journal homepage: www.elsevier.com/locate/nanoen

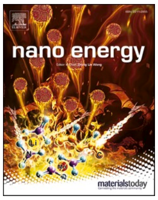

A multi-hole resonator enhanced acoustic energy harvester for ultra-high electrical output and machine-learning-assisted intelligent voice sensing

Guojian Zhu [a,b,1], Yi Zhou [c,1], Zeyu Si [d], Yin Cheng [a,*], Fei Wu [a,f], Huan Wang [e,f], Yaozong Pan [d], Jing Xie [e,f], Chaobo Li [e,f], Aiying Chen [b], Ranran Wang [a,g,**], Jing Sun [a]

[a] *The State Key Laboratory of High Performance Ceramics and Superfine Microstructure, Shanghai Institute of Ceramics, Chinese Academy of Science, Shanghai 200050, China*
[b] *School of Materials and Chemistry, University of Shanghai for Science and Technology, Shanghai 200093, China*
[c] *Department of Electrical and Computer Engineering, National University of Singapore, 4 Engineering Drive 3, Singapore 117583, Singapore*
[d] *Qingdao Branch of Institute of Acoustics, Chinese Academy of Sciences, Beijing 100190, China*
[e] *Institute of Microelectronics, Chinese Academy of Sciences, Beijing 100029, China*
[f] *University of Chinese Academy of Sciences, Beijing 100049, China*
[g] *School of Chemistry and Materials Science, Hangzhou Institute for Advanced Study, University of Chinese Academy of Sciences, 1 Sub-lane Xiangshan, Hangzhou 310024, China*

ARTICLE INFO

Keywords:
Triboelectric nanogenerator
Multi-Hole Acoustic Resonator
Acoustic-to-electricity conversion
Sound signal sensing
Machine learning

ABSTRACT

Acoustic energy harvesters are promising platforms for noise-to-electricity conversion in distributed environmental power supply and sound sensing in intuitive voice user interface. However, their efficacy in real-world applications is frustrated by the low electric output. We here report a multi-hole acoustic resonator enhanced triboelectric nanogenerator (MHAR-TENG) that couples a perforated plate resonator and a pressure differential acoustic receiver. It generated open-circuit voltage of 347 V, short-circuit current of 95 μA, and record-high power density of 8.9 W/m^2. The numerical simulation confirmed the sound pressure amplification for enhanced output performance. Besides, the high signal-to-noise ratio and precise high-frequency response of electrical signals enabled the high-quality restoration of music and human speech. Assisted by machine learning, the MHAR-TENG realized self-powered voiceprint identification and emotion recognition with a remarkably improved accuracy over 90 %. Our MHAR-TENG holds great potential for efficient acoustic-to-electrical conversion in the fields of noise recycling, biometric authentication, and human-machine interaction.

1. Introduction

With the arrival of the Internet of Things (IoT) and artificial intelligence (AI), sound waves in the environment will play an important role [1]. On one hand, acoustic energy, as a clean mechanical energy, can be converted into electricity, not only to solve the harmful noise issue, but also to power various terminal microelectronic devices of IoT in distributed environments [2,3]. On the other hand, human voice, encoded with rich biological information, has great potential for biometric authentication and human-machine interaction to fuel future AI [4–7]. However, the ubiquitous sound wave energy (its power on the order of milliwatts to watts [8]) is often ignored and wasted due to its low energy density and lack of effective collection methods. Currently, among the conventional acoustic energy harvesters: piezoelectric harvesters are limited by low electrical output performance and structural complexity; electromagnetic harvesters often require bulky components, such as coils and magnets, which deviates from the pursuit of lightweight [9–11]. Furthermore, the operating frequency of many devices usually falls within high levels around several kilohertz. Nonetheless, the sound sources in daily life are dominated by low-frequency ranges (20–200 Hz) from human speech, factory machines, site constructions and transportations [12,13], resulting in a low acoustic-to-electrical conversion efficiency. Therefore, a high-performance and widely deployable acoustic energy harvester that is suitable for low-frequency

---

* Corresponding author.
** Corresponding author at: The State Key Laboratory of High Performance Ceramics and Superfine Microstructure, Shanghai Institute of Ceramics, Chinese Academy of Science, Shanghai 200050, China.

E-mail addresses: chengyin@mail.sic.ac.cn (Y. Cheng), wangranran@mail.sic.ac.cn (R. Wang).

[1] These authors contributed equally: Guojian Zhu, Yi Zhou

https://doi.org/10.1016/j.nanoen.2023.108237
Received 19 October 2022; Received in revised form 15 January 2023; Accepted 27 January 2023

bands is highly demanded.

Triboelectric nanogenerators (TENG) is a feasible technology to convert low-frequency mechanical vibration into electrical energy [14]. Compared with piezoelectric and electromagnetic harvesters, TENG acoustic energy harvesters are usually much more cost-effective, simpler in structure, and exhibit superior energy-harvesting performance, making them promising in acoustic energy collection [15,16]. The TENGs for acoustic energy harvesting and sound wave sensing can be mainly divided into two types, i.e., non-resonant cavity and resonant cavity structures. Liu [17] developed a multi-layered structure of TENG, which can effectively improve the output performance through the parallel connection of multiple TENGs. Under the coordinated vibration of four units, its maximum short-circuit current can reach 2.1 mA. Qiu and coworkers [18] designed a sandwich-like sound-driven TENG based on Cu foam, polyvinylidene fluoride (PVDF) nanofibers and nylon fabric. The maximum current density of this sound-driven TENG is 25.01 mA/m^2 and the charging rate is 20.91 μC/s under 110 dB sound pressure level (SPL). However, due to the lack of resonant cavity to amplify the sound pressure, these sound-driven TENG devices have poor acoustic energy harvesting efficiency when there is a certain distance from the sound source. The sound wave propagating in the state of spherical wave will degrade rapidly in the air medium. With reference to Eq. (1), the intensity of spherical sound wave is inversely proportional to the square of the distance from the sound source. When the distance is doubled, the actual SPL is attenuated by 6 dB.

$$L_{p_1} - L_{p_2} = 20\lg\frac{r_1}{r_2} \tag{1}$$

Where r_1 and r_2 are the distances from position 1 and position 2 to the sound source, respectively. For this reason, Zhao et al. [19] investigated a dual-tube Helmholtz resonator-based triboelectric nanogenerator (HR-TENG). Under the optimal output frequency of 70 Hz and SPL of 85.3 dB, its open circuit voltage and short circuit current can reach 132 V and 32 μA, respectively. However, the HR-TENG has low output power and sensing performance when it comes to self-powered speech recognition. A quarter-wavelength acoustic resonator system was proposed for high performance acoustic energy scavenging [20]. Nonetheless, the bulky aluminum tube with a length of 0.94 m and a radius of 50 mm for acoustic transmission limits its application scope. Xu successfully developed high-performance acoustic TENG devices with sound pressure enhancing effect based on multi-tube [21] or coniform tube [22] resonators. However, the convenient and accurate sound sensing, especially voice-related sensing, which demands high electric output with excellent signal-to-noise ratio, still needs to be addressed. In general, TENG device that combines efficient low-frequency sound energy harvesting with superb sound sensing capability is still a formidable challenge.

Herein, we report a multi-hole acoustic resonator enhanced triboelectric nanogenerator (MHAR-TENG) that combines high power density with intelligent sound signal sensing. The MHAR-TENG is designed by coupling the perforated plate resonator and the pressure differential acoustic receiver. It can produce high electrical output and exhibit excellent sound sensing ability through the combination of sound pressure amplification effect and proximity effect. The advantages of the MHAR-TENG are proved theoretically and experimentally. Under 150 Hz and 104 dB sound wave excitation, the MHAR-TENG generates open-circuit voltage (V_{OC}) of 347.3 V, short-circuit current (I_{SC}) of 95.8 μA and transfer charge (Q_{SC}) of 292.8 nC. Under the same excitation, the maximum charging rate of the MHAR-TENG is 31.9 μC/s and its instantaneous power density is 8.9 W/m^2, which are higher than those of previously reported sound-driven TENG and PENG (Piezoelectric Nanogenerator) devices. In addition, the MHAR-TENG can not only power miniature electronic devices, but also work as a self-powered sound signal sensor. Assisted by machine learning analysis technology, MHAR-TENG realizes the recognition of individual voiceprint, and the classification of various voice emotions of a single person, which is not reported before to the best of our knowledge. The recognition accuracy of the MHAR-TENG is over 90 %, while that of the acoustic TENG without a muti holes resonator is only 26 %. In general, this work provides a new model for the large-scale application of future acoustic-to-electrical conversion in the fields of noise recycling, military monitoring, and acoustic human-machine interaction [23–25].

2. Results and discussion

As shown in Fig. 1a, the MHAR-TENG consists of an acoustic resonant cavity based on a perforated plate and an acoustic TENG. The detailed layer-by-layer structural scheme of the acoustic TENG is shown in Fig. 1b. It is composed of a conductive fabric, a spacer with the thickness of 70 μm, PVDF nanofiber film, a commercial PE film and Al electrode. The SEM image of PVDF nanofibers is shown in the Fig. 1c. The PVDF nanofibers were fabricated by electrospinning, which is propitious to the polarization of PVDF molecules (schematic of the electrospinning setup in Supplementary Fig. S1). The prepared nanofibers have a smooth surface without beads, and the average diameter is between 400 and 900 nm. The fibrous microstructure of PVDF films can greatly increase the contact area with the conductive fabric in the contact mode, thereby facilitating the charge transfer [26]. The inherent air-permeable microporous structure of the fabric is beneficial to the transmission of sound waves, as shown in Fig. 1d. In order to transfer charges instantly to the external circuit, the Al electrode with a thickness of 90 nm is pre-deposited on one side of the PE film via magnetron Sputtering (Supplementary Fig. S2). The detailed device fabrication process is described in Experimental Section. Fig. 1e shows the front and back of the MHAR-TENG. The size of the acoustic TENG and the resonant cavity is well matched, which is beneficial to the full utilization of incident sound wave and the formation of internal and external sound pressure differences.

The structural design of the MHAR-TENG combines the principle of perforated plate and the advantages of the pressure differential acoustic receiver model, which plays a vital role in the resonant absorption of low-frequency sound waves. A receiver based on the principle of the pressure difference between two adjacent points in the sound field is called a pressure differential receiver. The front and the back sides of the vibrating film are located at different positions within the sound field, which leads to a net sound pressure difference exerted on the film due to the varied sound pressure intensity at the two individual sides. Such desired pressure difference drives the vibration of the flexible film. On one hand, as a classical resonant sound absorption structure, perforated plate is actually composed of many parallel cavity resonators (Helmholtz resonators), which can be used to concentrate acoustic energy and amplify sound pressure [27] (Fig. 1f). On the other hand, the pressure differential acoustic receiver almost only responds to the incident sound wave from the front hemisphere, so it is used as a sound signal sensor. Such proximity effect can eliminate noise interference from other directions, enabling reliable sound sensing applications [28].

After the acoustic TENG is placed inside the resonant cavity, the PE film would vibrate when the TENG is triggered by an external sound wave excitation. Fig. 1g schematically depicts the working mechanism of the acoustic TENG. At the beginning, the PVDF film with strong electronegativity would attract free electrons from the bottom conductive fabric upon contact [29]. Subsequently, the vibrating film separates from the bottom electrode under the action of sound pressure, resulting in the separation of positive and negative triboelectric charges and a potential difference between the two electrodes. The negative charge, driven by the potential difference, flows from the aluminum electrode to the fabric electrode through an external circuit to balance the local electric field and generate a pulsed current. At the maximum separation displacement, the electrostatic equilibrium is established and the charge flowing stops. As the vibrating film approaches the bottom electrode, the potential difference gradually decreases and current of opposite

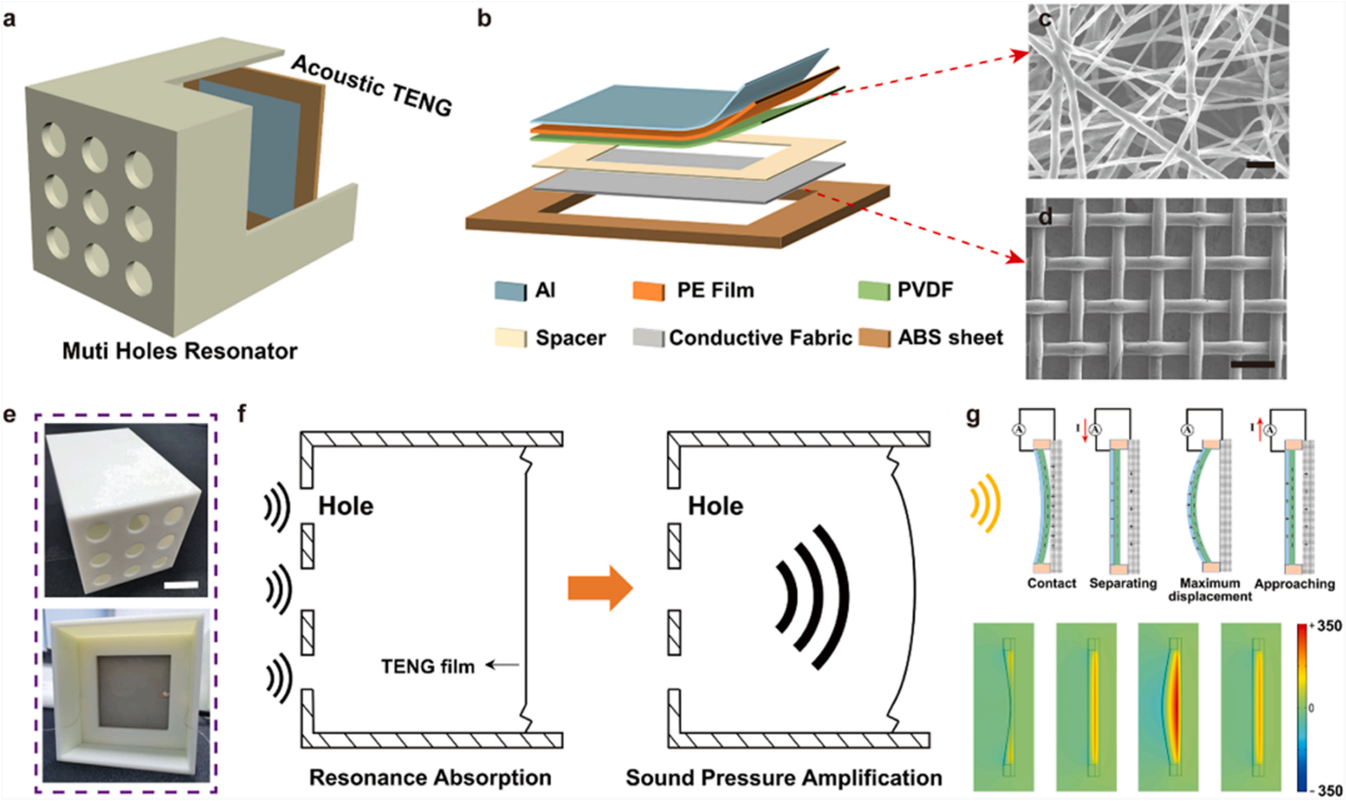

Fig. 1. Structure and mechanism of the MHAR-TENG. a Structure scheme of the MHAR-TENG. b Schematic diagram of the acoustic TENG without the resonant cavity. c SEM image of the PVDF nanofibers. Scale bar, 2 μm. d SEM image of the conductive fabric. Scale bar, 200 μm. e Optical photograph of the MHAR-TENG. Scale bar, 2 cm. f Schematic diagram of sound pressure amplification of the MHAR-TENG. g Working mechanism of the acoustic TENG and the COMSOL simulation of periodic potential variation between two electrodes of the acoustic TENG.

direction is generated. In order to further confirm the working principle of the acoustic TENG, Fig. 1g shows the simulation results of potential distribution of the MHAR-TENG.

First, we compared the output performance difference of the MHAR-TENG and the acoustic TENG without a multi-hole resonator. The test frequency range is 50–170 Hz, and the sound pressure level ranges from 54.8 to 100.1 dB. In this part, a loudspeaker is used to provide a sine wave, and the frequency or amplitude of the sound wave are adjusted by an audio signal generator. During the test, a foam plate is placed under the MHAR-TENG to prevent the vibration caused by the loudspeaker from being transmitted through the table, which will interfere with the test results (Supplementary Fig. S3). The V_{OC} of the acoustic TENG and the MHAR-TENG under the same excitation of sound waves is displayed in Fig. 2a. The trend of their output performance with frequency is similar. The V_{OC} of TENG and MHAR-TENG increases gradually with acoustic frequency and reaches peak value at 100 Hz and 150 Hz respectively, after which, the Voc of both devices decreases sharply and then stabilizes at a very low value. Although they show similar output trend with frequency, the output performance of the MHAR-TENG is much higher than that of acoustic TENG in the whole test frequency range. The peak Voc of the MHAR-TENG is 314 V, around 3 times higher than that of the acoustic TENG, which is only 77.4 V. Similarly, the peak Isc of MHAR-TENG is 95.54 μA, 4.6 times higher than that of the acoustic TENG, which is 17.02 μA, as shown in Supplementary Fig. S4. Under acoustic excitation of maximum amplitude, the resonance frequency band of the MHAR-TENG is notably broadened. For example, for the MHAR-TENG, the resonance frequency range for V_{OC} higher than 60 V, is 50–150 Hz. While the range is much smaller for the acoustic conventional TENG, being from 90 to 120 Hz. Also, we found that the TENG with a fully opened resonator (no holes) exhibited similar output performance to that of a single TENG device in air, which verified the acoustic energy enhancing effect of the perforated plate with designed holes.

The superior output performance is attributed to the enhancement of the harvested acoustic energy in resonant cavity. Actually, the conventional perforated plate resonators can be regarded as a set of mass-spring resonance system [30]: The air vibrates with sound waves in the holes like a sound quality element; The pressure in the cavity changes with the expansion and contraction of the air like a spring. When the frequency of the incident sound wave matches the resonance frequency of the system, the air at the holes generates intense vibration and friction, which strengthens the resonant absorption effect, forms an absorption peak, and significantly increases the acoustic energy in the cavity. On the contrary, when it is far from the resonance frequency, the sound pressure amplification effect weakens gradually [31]. Based on ANSYS simulation modeling, two-dimensional cross-sectional view of sound pressure distribution map of the MHAR-TENG under an acoustic frequency of 150 Hz is obtained, as shown in Fig. 2b. The result shows that the maximum sound pressure is located at the sound source, and the sound pressure decreases rapidly as the sound wave propagates outwards. While within the same radius, the sound pressure inside the resonator is obviously higher than that outside.

By adjusting the structural parameters of the resonant cavity, we can broaden the acoustic resonance frequency band and enhance the sound absorption effect. The resonance frequency of the perforated plate is calculated as follow [32]:

$$f_0 = \frac{c}{2\pi}\sqrt{\frac{P}{(t+0.8d)L}} \tag{2}$$

where L is the thickness of the air layer behind the plate, t the thickness of the plate, d the hole diameter, c the speed of sound, and P the

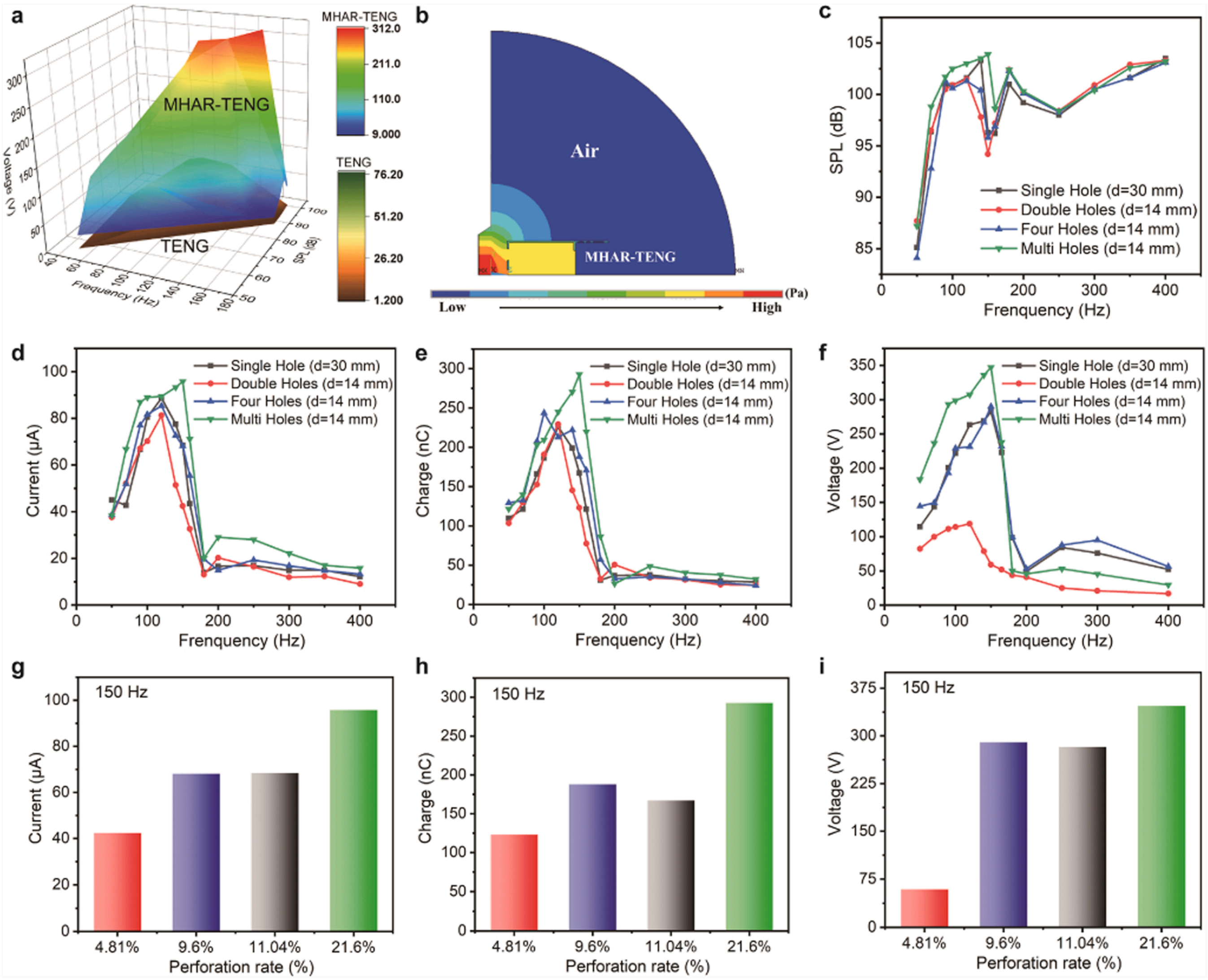

Fig. 2. Influence of the structural parameters on the output power performance of the MHAR-TENG. a V_{OC} of the acoustic TENG and the MHAR-TENG under the same excitation of sound waves with frequencies ranging from 50 to 170 Hz. b Two-dimensional cross-sectional view of sound pressure distribution map of the MHAR-TENG under an acoustic frequency of 150 Hz. c The measured SPLs for several NHAR-TENGs under the excitation of sound waves with frequencies ranging from 50 to 400 Hz. d I_{SC}, e Q_{SC} and f V_{OC} of NHAR-TENGS vary with frequencies ranging from 50 to 400 Hz when changing perforation rate. Comparison of g I_{SC}, h Q_{SC} and i V_{OC} of NHAR-TENGS under an acoustic frequency of 150 Hz.

perforation rate (perforation area/full area). From Eq. (2), P and d are the main influencing factors of the perforated panel resonance frequency. Therefore, we combined the acoustic TENG and the resonant cavities with different P and d to form NHAR-TENGs (N in “NHAR-TENGs” represents the number of holes), so as to investigate the impact of perforation rate on the output performance. The photos of resonant cavities with different perforation rates are shown in Supplementary Fig. S5. When other parameters such as volume and wall thickness are the same, the perforation rate of the resonant cavity increases from 4.81 % (double holes acoustic resonator-TENG) to 9.6% (four holes acoustic resonator-TENG), 11.04 % (single hole acoustic resonator-TENG) and 21.6 % (MHAR-TENG). The holes are arranged in an axisymmetric manner, and each resonant cavity is 3D printed with the same UV Curable Resin material.

Sound pressure level (SPL) is a logarithmic measure of the effective pressure of a sound relative to a reference value, also the most used indicator of the acoustic wave strength. The SPL values within TENGs under the same excitation conditions can be adopted to assess the sound wave enhancing effect of the resonators. Further characterization examined the detailed relationship between SPLs of NHAR-TENGs and perforation rate, as shown in Fig. 2c. In the resonance frequency range of 50–150 Hz, the SPL of the MHAR-TENG is slightly higher than that of other NHAR-TENGs under the same excitation, which proves that it has the strongest sound pressure amplification effect. The maximum SPL of the MHAR-TENG (104 dB,150 Hz) is higher than that of DHAR-TENG (101.5 dB,120 Hz), FHAR-TENG (101.3 dB,120 Hz), SHAR-TENG (103.3 dB,140 Hz). Above 200 Hz, the SPL difference of the NHAR-TENGs can be neglected since the resonance effect is very weak in this range.

Fig. 2d-f shows the I_{SC}, Q_{SC}, and V_{OC} of NHAR-TENGs with different perforation rates and their effective acoustic resonance frequency is concentrated within 50–200 Hz. In this resonance frequency range, the overall output performance of the MHAR-TENG is higher than that of other NHAR-TENGs at each frequency under the same excitation of sound waves. Besides, each curve has a significant performance degradation beyond the optimal output frequency. The optimal output frequency of NHAR-TENGs changes from 120 to 150 Hz with the increase of the perforation rate, which accords with the law described in Eq. (2). In fact, according to Eq. (2), the theoretical resonance frequencies of NHAR-TENGs are 116.9 Hz for DHAR-TENGs, 165.2 Hz for FHAR-

TENG, 126.3 Hz for SHAR-TENG and 247.8 Hz for MHAR-TENG, respectively. The insignificant deviation between the measured and theoretical resonance frequencies is because that NHAR-TENGs are not a completely perforated plate structure and the boundary consistency of the NHAR-TENGs is destroyed by the existence of the flexible film. As shown in Fig. 2g-i, the short-circuit current increases from 42.42 to 95.84 μA, the transfer charge from 123.12 to 292.85 nC and the open-circuit voltage from 118.84 to 347.31 V, as the perforation rate increases from 4.81 % to 21.6 % under 150 Hz sound wave excitation. The increase is 55.74 %, 57.96 % and 65.78 %, respectively. It is worth noting that the output performance of FHAR-TENG and SHAR-TENG is basically the same in the frequency range from 50 to 400 Hz when the hole diameter is different but the perforation rate is similar, as shown in Fig. 2d-f and Fig. 2g-i.

Hence, it can be concluded that the sound pressure amplification effect is stronger with a higher perforation rate. Specifically, when the sound wave propagates to the hole, the wave at the hole is regarded as a new independent wave source. The increase in the number of independent wave sources causes the superposition of the sound waves passing through different holes, which enhances the pressure in the cavity. Taking the superposition of two series of waves as an example, suppose that the sound wave emitted by the loudspeaker passes through the holes of the resonant cavity to form two series of sound waves of the same frequency. Their sound pressure is p_1 and p_2, respectively, and the sound pressure of their synthesized sound field is p, which all satisfies the basic wave equation:

$$\nabla^2 p = \frac{1}{c_0^2}\frac{\partial^2 p}{\partial t^2}\nabla^2 p_1 = \frac{1}{c_0^2}\frac{\partial^2 p_1}{\partial t^2}\nabla^2 p_2 = \frac{1}{c_0^2}\frac{\partial^2 p_2}{\partial t^2} \tag{3}$$

Add the above two equations, since each equation is linear:

$$(p_1 + p_2) = \frac{1}{c_0^2}\frac{\partial^2 (p_1 + p_2)}{\partial t^2} \tag{4}$$

Comparing Eqs. (3) and (4), and considering that the acoustic boundary conditions are also linear:

$$p = p_1 + p_2 \tag{5}$$

Therefore, the sound pressure synthesized by two waves is equal to the sum of the sound pressure of each wave, which is called the principle of acoustic superposition. This conclusion can be extended to the simultaneous existence of multiple acoustic waves. In all, compared with other perforated resonators with less holes, the multi-hole acoustic resonator exhibited higher electrical output performance and broader half-peak width of the resonant band, which conforms to the principle of acoustic superposition. The MHAR-TENG was further systematically investigated for optimized performance.

Frequency and amplitude are basic parameters to describe acoustic characteristics. To investigate the impact of the amplitude of the sound wave on the output performance of the MHAR-TENG, we fixed the frequency of the audio signal generator at 150 Hz, adjusted its output voltage amplitude to change the SPL of the sound wave, and collected the V_{OC} and I_{SC} of the MHAR-TENG as exhibited in Fig. 3a, b. As the SPL increases from 70 to 104 dB, the V_{OC} and I_{SC} increased evidently from 10 to 340 V, and 2.7–95 μA, respectively. It is worth noting that the increment of voltage is not obvious when the SPL is in the range of 70 dB~82 dB. However, when the SPL is in the range of 82 dB~104 dB, the voltage increments almost double for every 6 dB increment, and the growth trend of current is similar. According to previous reports [33,34], the open-circuit voltage of the MHAR-TENG can be calculated as following:

$$V_{OC} = \frac{\sigma x(t)}{\varepsilon_0} \tag{6}$$

Here σ is the charge density, $x(t)$ the separation displacement of the PE film, and $\varepsilon_0$the dielectric constant. Therefore, at same frequency, the increase in sound pressure makes the film vertical displacement and

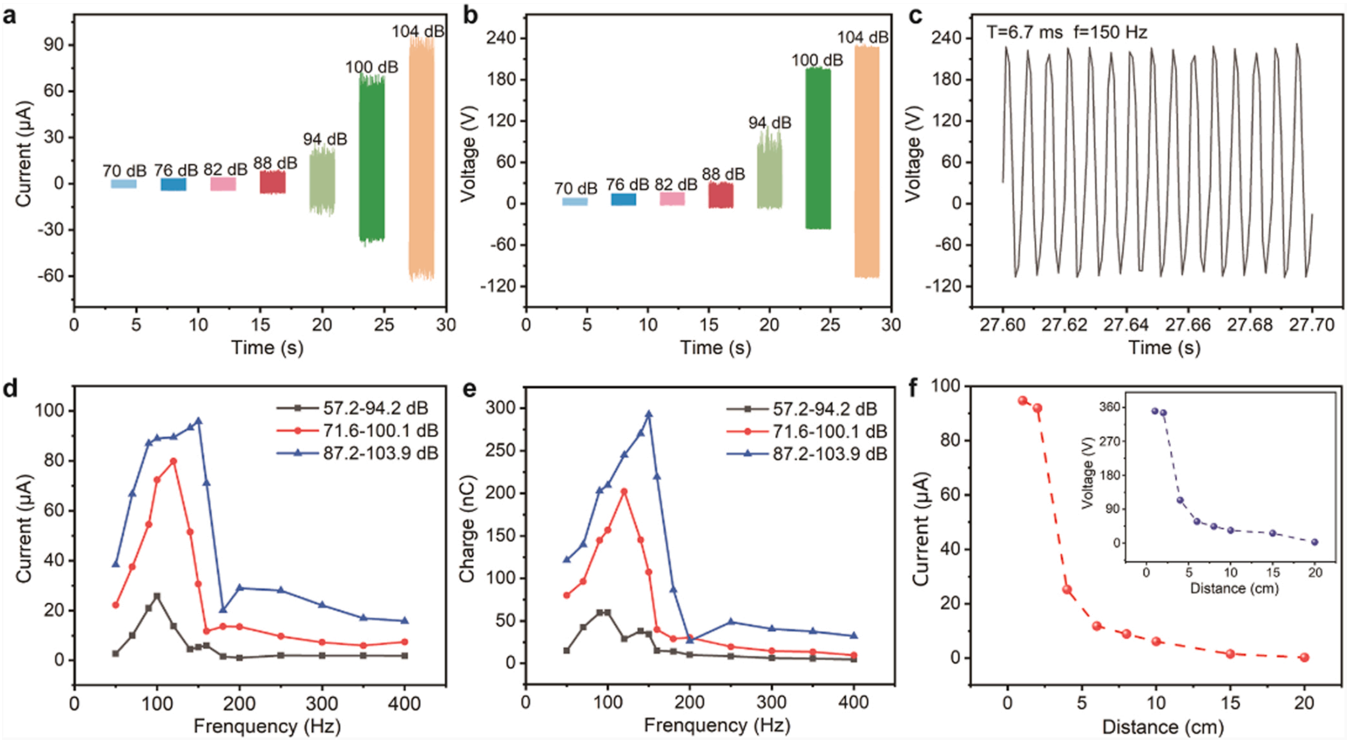

Fig. 3. Influence of the acoustic parameters on the output power performance of the MHAR-TENG. a V_{OC} and b I_{SC} of the MHAR-TENG under sound with 150 Hz and different SPLs ranging from 70 dB to 104 dB. c Enlarged view of the V_{OC} of the MHAR-TENG under frequency of 150 Hz and SPL of 104 dB. d I_{SC} and e Q_{SC} of the MHAR-TENG under different amplitude sound wave excitation with frequencies ranging from 50 to 400 Hz. f The MHAR-TENG is used as a sound wave sensor for distance detection of environmental sound sources.

contact area increase gradually, resulting in higher electrical output. In addition, as shown in Figure3c, the period between the voltage peaks is 6.7 ms, which clearly matches the acoustic excitation frequency of 150 Hz, indicating that the MHAR-TENG has precise frequency response, which is particularly important in audio signal sensing applications.

At the same time, Fig. 3d and Fig. 3e depict the relationship between the I_{SC}, Q_{SC} and frequency of the MHAR-TENG under different sound wave amplitudes, respectively. We used an audio signal generator to adjust the sound wave amplitude (input voltages of 3, 7, and 18 V to the generator for comparative testing), and the SPLs at the same frequency ranged from 57.2 dB to 94.2 dB, 71.6–100.1 dB, 87.2–103.9 dB, respectively. As the amplitude of the sound wave increases, the peak electrical output increases significantly. For example, the I_{SC} increased from 25.8 to 95.8 μA. It is interesting that the optimal output frequency of the MHAR-TENG increases gradually as the amplitude increases. The optimal output frequencies are 100, 120, and 150 Hz at input voltages of 3, 7, and 18 V, respectively. The main reason for this phenomenon is the change of sound wave energy. Sound intensity (I) is a characteristic parameter describing the energy passing through a unit area perpendicular to the direction of sound wave propagation, which is defined as:

$$I = \frac{1}{2}\rho c \omega^2 A^2 \tag{7}$$

wherein ρ is the density of the medium, ω the angular frequency, c the speed of sound, and A the amplitude of the sound wave. Eq. (7) indicates that the sound intensity is proportional to the square of the amplitude. At the same frequency, the sound wave with small amplitude generates lower energy. As a result, the contact-separation process of the vibrating membrane driven by small amplitude acoustic wave is not sufficient. The displacement and contact area decrease, and the electrical output performance declines accordingly. In addition, the optimal output frequency decreases as the amplitude of the sound wave decreases. Therefore, it can be concluded that the optimal output frequency of the MHAR-TENG, also known as the resonance frequency, is determined by the external sound wave excitation and its structure. We further evaluated how the distance from the MHAR-TENG to the sound source affect the output signal. At a fixed frequency of 150 Hz, the electrical output is measured in Fig. 3f. The I_{SC} decreased from 94.7 to 0.21 μA, V_{OC} from 350 to 2.59 V, when the distance increased from 1 to 20 cm. Through such a test, a quantitative model of the MHAR-TENG for distance detection of forward sound sources can be established.

Power density is an important performance indicator for evaluating acoustic energy harvester. As shown in Fig. 4a, with the increase of the

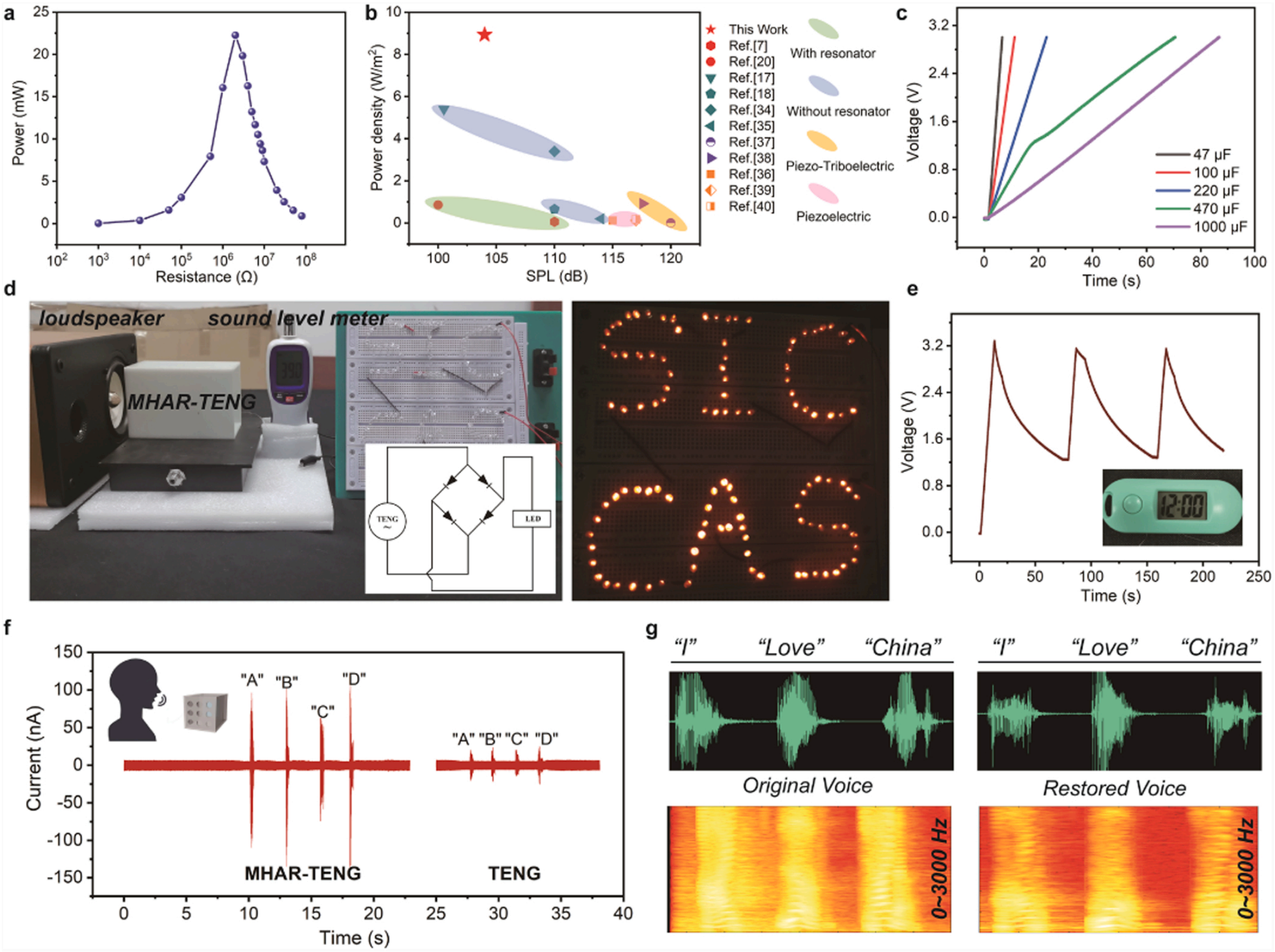

Fig. 4. The MHAR-TENG as a sustainable power source and for sound signal sensing. a Dependence of the output power on the external load resistance. b Output power density compared with reported works. c Charging of different capacitors by the MHAR-TENG electrical output under frequency of 150 Hz and SPL of 104 dB. d Photograph of "SICCAS" composed of LED lights are directly lit up by the MHAR-TENG and its circuit diagram. e Experimental graph of the power supply for a small electronic clock; after the 100 μF capacitor is charged to 3 V. f The MHAR-TENG and the acoustic TENG are used for simple human voice signal detection. g The time-domain sound wave signal (top) and spectrograms(bottom) of original voice and restored voice.

external loading resistance, the instantaneous output power first increases and then decreases under 150 Hz and 104 dB sound wave excitation. The instantaneous output power reaches the maximum value of 22.27 mW at optimal external resistance of 2 MΩ. Furthermore, Fig. 4b shows the output power density of the MHAR-TENG (8.9 W/m^2) is not only much higher than those of the piezoelectric or piezo-triboelectric nanogenerators, but also superior to those of sound-driven TENGs with resonators reported previously [3,17,18,20,35–42]. The principle of acoustic superposition and the sound pressure amplification effect synergistically promote the concentration of acoustic energy in MHAR-TENG and improve the electrical output performance. The specific data of different works are shown in Supplementary Table 1. The higher power density achieved at lower SPL, fully endows the MHAR-TENG with huge advantage in acoustic-to-electricity conversion.

The high output power density imparts good charging ability to the MHAR-TENG. Fig. 4c shows the charging curves of the MHAR-TENG for different capacitors under 150 Hz, 104 dB sound wave excitation. The 47 μF capacitor is charged from 0 to 3 V within only approximately 6.69 s, whereas about 86.85 s are required for a 1000 μF capacitor. Besides, charging curves of a 100 μF capacitor at different frequencies is shown in Supplementary Fig. S6a. The results indicate that the charging speed of 100 μF capacitor increases first and then decreases with the change of acoustic frequency. The actual measured charging rate is calculated from the charging curve and plotted in Supplementary Fig. S6b. Under the excitation of 150 Hz sound wave, a 100 μF capacitor can be charged to above 7 V in 22 s and the maximum charging rate of MHAR-TENG reaches 31.9 μC/s. Such a charging rate has a significant improvement compared to other sound-driven TENGs with the same effective working area [18,19,35].

In order to verify the actual power supply utility, we connected the MHAR-TENG to a full-wave rectifier bridge, and the output energy is directly supplied to the LEDs. Fig. 4d shows the digital photo and circuit diagram of lighting LEDs, and all the LEDs in the word “SICCAS” could be easily lit up driven by sound wave with the frequency of 150 Hz and SPL of 104 dB (Supplementary Movie S1). Under the same sound pressure level, the 100 μF capacitor was quickly charged to 3 V and successfully powered the electronic clock continuously, as depicted in Fig. 4e and Supplementary Movie S2.

Supplementary material related to this article can be found online at doi:10.1016/j.nanoen.2023.108237.

In addition, due to the accurate frequency resolution and proximity effect, the MHAR-TENG can also be utilized as a self-powered sound sensor. On one hand, as shown in Fig. 4f, one volunteer spoke the letters "A", "B", "C" and "D" to the MHAR-TENG and the control acoustic TENG, using the same speech speed and volume. Compared with the acoustic TENG, the MHAR-TENG can amplify the received vocal signal strength significantly. The signal amplitude of "A", "B", "C" and "D" increased from 20 nA to more than 100 nA. On the other hand, as the loudspeaker played a part of the pure music “summer”, the MHAR-TENG converted the music signal into current signal from the loudspeaker (distance of 20 cm). Current signals with high signal-to-noise ratio and superb fidelity can be easily obtained without the need of complicated signal post-processing. Subsequently, the current waveform was restored to music simply after filtering noise by MATLAB software. The restored music sounded almost the same as the original music (signal recording and restoration in Supplementary Movie S3). The time-domain sound wave signal, and spectrograms of original and restored music are shown in Supplementary Fig. S7, respectively. Program written in MATLAB is shown as Supplementary Note 1. Not only music, but a speech sentence “*I love China*” played by the loudspeaker can also be directly recorded and clearly restored by the MHAR-TENG. As show in Fig. 4g, the similar time-domain sound wave signal, and spectrograms of the original and restored voice, indicate that the MHAR-TENG has the potential to work as an efficient self-powered sound sensor.

Supplementary material related to this article can be found online at doi:10.1016/j.nanoen.2023.108237.

The above work shows that the proposed MHAR-TENG can accurately perceive and record human voice signals, suggesting a powerful tool for artificial intelligent speech interaction. Besides, machine learning technology can provide an effective method to automatically learn representative features from the collected original signals, and has made great achievements in audio analysis [4]. When the MHAR-TENG is combined with machine learning auxiliary signal analysis technology, an intelligent sound signal analysis platform can be developed for voiceprint identification and emotion recognition. The structure and data process flow of the MHAR-TENG for individual voice physiology recognition is shown in Fig. 5a. Upon the excitation of utterance, the generated charge, current, and voltage signals from the MHAR-TENG are acquired by the signal acquisition module in a real-time manner. Fig. 5b schematically shows the individual voiceprint identification through machine-learning assisted MHAR-TENG. Specifically, 60,000 samples in charge, current, and voltage channels (marked as one group) were collected separately for each user when speaking a sentence “Open the door, please”. Then, a whole dataset was built from 8 different users (5 male and 3 female). There are 4 groups of data in total used for analysis: 3 groups for training, and 1 for prediction. The output raw signals for each user’s voice are shown in Supplementary Fig. S8, while the recorded voice for 8 different users is shown in Supplementary Movie S4.

Supplementary material related to this article can be found online at doi:10.1016/j.nanoen.2023.108237.

In this study, the data training model used in the system were configured as follows: the principal component analysis (PCA) was used to implement the features for training, the Ensemble classifier (Bagged Trees) was used for data classification, and the confusion chart was obtained after training, as shown in Fig. 5c. It was observed that the trained model was able to distinguish the different voiceprint of eight users with accuracy of 92.7 %. For comparison, the same voiceprint recognition training procedure was performed to the conventional acoustic TENG as control group. The corresponding signal patterns of 8 different users and the predicted results are shown in supplementary Fig. S9, showing a recognition accuracy of only 26 %. Fig. 5d provides the accuracy comparison of conventional TENG and MHAR-TENG for 8 different users in voiceprint identification using the same processing protocol. The results confirm the accuracy of the individual voiceprint recognition can be improved considerably, which can be attributed to the sound pressure amplification capability and sound receiving structure of the MHAR-TENG.

Fig. 5e shows schematic process of the emotion recognition through machine-learning assisted MHAR-TENG. 60,000 samples in charge, current and voltage channels (marked as one group) were collected separately for one user when speaking a sentence “I feel good” in angry, happy, and sad moods. The user was required to express the emotional characteristics in the uttered words for effective classification. 4 groups of data in total were collected: 3 groups for training, and 1 for prediction. The output charge, current, and voltage signals collected when the user’s voice is played is shown in Fig. 5f, while the recorded voice of the user is shown in Supplementary Movie S5. The flow chart and classifier remained consistent with the voiceprint recognition. The prediction data analyzed with emotion trained model was used for accuracy calculation and plotting confusion map in Fig. 5g. The average recognition accuracy is 93.6 %, providing great potential for high-accuracy emotion recognition based on machine learning prediction.

Supplementary material related to this article can be found online at doi:10.1016/j.nanoen.2023.108237.

Overall, in these intelligent voice sensing demonstrations, the unique voiceprint of different individuals and the emotional information contained in the speech can be successfully recognized, demonstrating the potential of the MHAR-TENG in the secure unlocking of voiceprints and intelligent human-computer interaction.

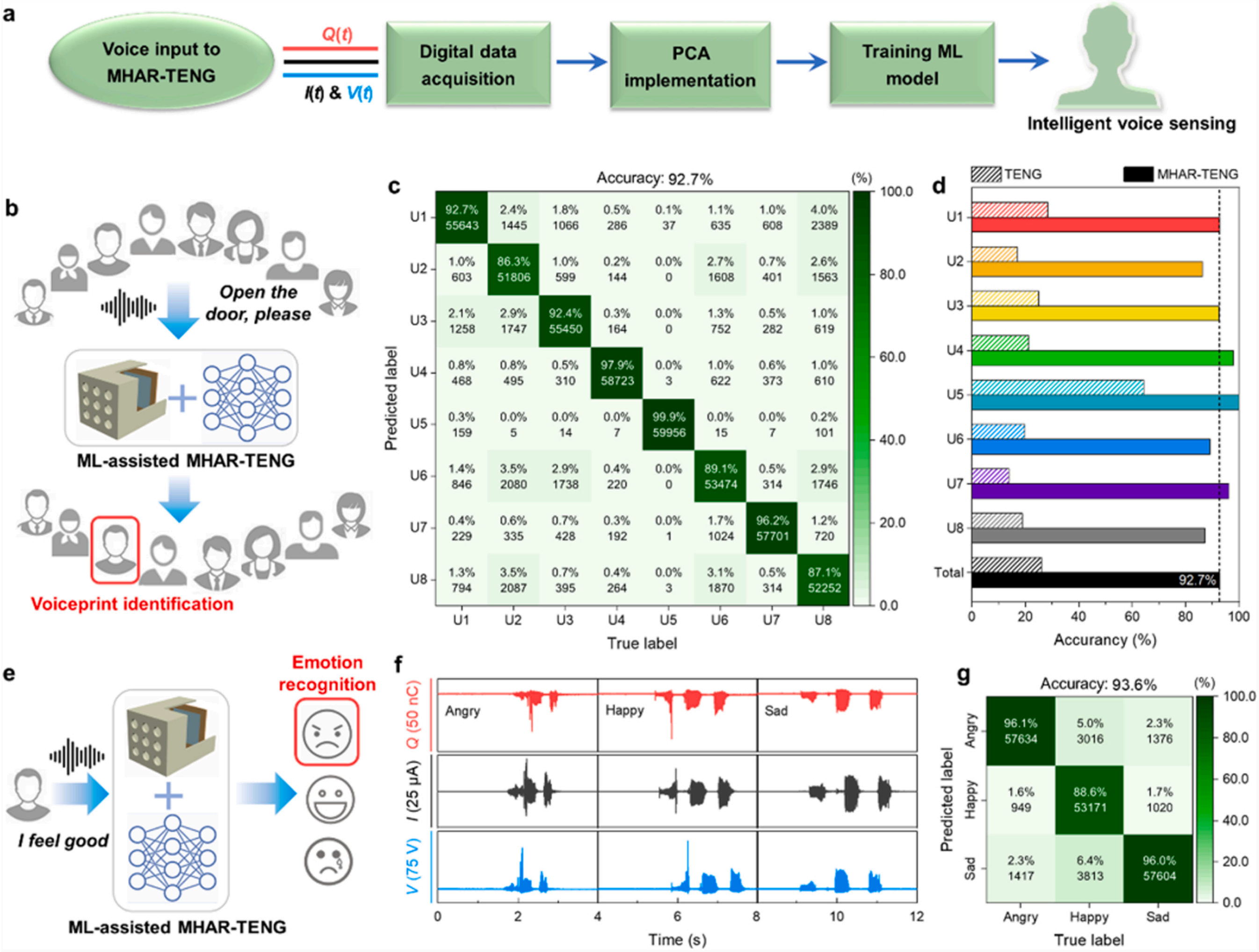

Fig. 5. Intelligent voice sensing via machine-learning assisted MHAR-TENG. a The structure and data process flow of the MHAR-TENG for individual voice physiology recognition. b Schematic diagram of the voiceprint identification process. c The confusion map of voiceprint recognition results. d Accuracy comparison of conventional TENG and MHAR-TENG in voiceprint identification. e Schematic diagram of the emotion recognition. f Charge, current and voltage plots for one user when speaking "I feel good" under different emotions of being angry, happy, and sad. g The confusion map of emotion recognition results.

3. Conclusion

In summary, we propose an acoustic energy harvester MHAR-TENG, which consists of an acoustic TENG and a 3D-printed muti-hole acoustic resonator. The MHAR-TENG based on the coupling of a perforated plate resonator and a pressure differential acoustic receiver exhibits excellent acoustic-to-electrical conversion and sound signal sensing capabilities. Compared with the acoustic TENG without the resonator, the MHAR-TENG has a much higher output performance, with the maximum output voltage and current increasing by 3and 4.6 times, respectively. Under the optimal frequency of 150 Hz and SPL of 104 dB, the open-circuit voltage and short-circuit current can reach 347.31 V and 95.84 μA, respectively. Further, we found that, the increase of the perforation rate of the resonant cavity allows the sound waves passing through the different holes to be superimposed on each other to form a synthesized sound field, which can effectively improve the sound pressure in the cavity and the electrical output performance of the MHAR-TENG. The MHAR-TENG shows ultrahigh output performance and application potential in acoustic energy harvesting. The charging speed for capacitors can reach 31.9 μC/s, and the maximum instantaneous power density is 8.9 W/m^2, which is higher than sound-driven TENG devices previously reported. Moreover, combined with machine learning technology, the MHAR-TENG can be used as a self-powered intelligent sound signal analysis platform for individual voiceprint identification and emotion recognition, with an accuracy of over 90%, much higher than a conventional sound-driven TENG. As an advanced acoustic energy harvester, the MHAR-TENG provides a new model for the large-scale utilization of acoustic energy and sound sensing in the future.

4. Experimental section

4.1. Fabrication of the PVDF nanofibers membrane

First, 1.08 g PVDF, 2.82 g N, N-dimethylformamide (DMF) and 5.10 g acetone were mixed in a 50 ml triangular flask. Then the homogeneous PVDF solution was vigorously stirred at room temperature for 4 h. Next, the solution was heat in oil bath for 30 min at 60 °C, which is favorable to avoid the generation of bead in the as-fabricated nanofibers. To begin with electrospinning, the uniform solution was added into a 5 ml syringe with a 25-gauge stainless-steel needle. And the electrospinning process was performed under the applied positive high voltage of 16 kV, spinning distance of 13 cm, and feed rate of 2.4 ml/h. The surface of the grounded rotating drum (250 rpm) was covered with a piece of PE film for collecting the PVDF nanofibers. Electrospinning time lasts for 15 min. Finally, the PVDF nanofibers were dried at 60 °C for 6 h in a vacuum drying oven.

4.2. Fabrication of the multi-hole acoustic resonator-triboelectric nanogenerator

The fabrication process of the MHAR-TENG can be divided into printing of the acoustic resonant cavity, the preparation of the acoustic TENG, and assembly of devices. The volume of the resonant cavity is 80 × 80 × 120 mm, and it was printed by a 3D printer with UV Curable Resin material. The printed shell with UV Curable Resin has a smooth surface, good toughness and high strength, which is also good for reflection and resonance of sound waves. The resonant cavity can be printed using a high-precision 3D printer to produce different acoustic hole structures for the convenience of comparison experiments. Typically, a piece of 3 mm thick square ABS sheet, which has a hollow structure with an inner diameter of 50 mm and outer diameter of 74 mm, was served as supporting substrate of the acoustic TENG. Then, A piece of conductive fabric (60 × 60 mm) was attached flat to the substrate along the four edges of the inner diameter to act as the bottom electrode. The conductive fabric (MF32D, purchased from Saintyear Electronic Technology Co., LTD.) was polyester mesh coated with copper-nickel metal layer on the surface, which has low surface resistance ($\leq$0.1 Ω/sq), good light and air permeability. Next, a double-sided tape used as spacer layer was adhered to the four edges of the conductive fabric, and the PE film was chosen as the vibrating membrane of the device, whose one surface is deposited with Al layer and the other surface is covered with PVDF nanofiber film to work as the tribo-layer. The thickness of the spacer was tuned to be 70 μm for optimized vibration space. Thus, the acoustic TENG was fabricated. The effective working area of the TENG was about 25 cm^2. Finally, the acoustic TENG was nested into the resonant cavity at a depth of 8 cm to form the MHAR-TENG. To ensure the maximum acoustic energy utilization, the TENG and the 3D resonator should be tightly assembled and the TENG needs to be parallel to the cavity perforation surface.

4.3. Characterization and electrical output measurement

The surface morphology of PVDF nanofiber and conductive fabric was characterized by SU8220 field emission scanning electron microscope. When measuring the electrical output, a loudspeaker driven by an audio signal generator (RK1212D) faced the MHAR-TENG. A sound level meter (GM1353) was used to record the sound wave pressure, which accuracy and resolution are 1.5 dB and 0.1 dB, respectively. Pure music and human voice were played through the loudspeaker connected to a power amplifier (SA-5016). The output signals, including the open-circuit voltage, short-circuit current, and transferred charges, were measured by a Keithley 6514 electrometer.

4.4. Finite element analysis of triboelectrics

The electrical potential profiles of MHAR-TENG were performed by the finite element method using COMSOL Multiphysics with an Electrostatic module. The measured TENG dimension and other parameters selected from the COMSOL materials library were utilized in the simulation. The triboelectric charge densities of PVDF thin film and conductive fabrics are fixed at $-$ 10 $\mu\text{C/m}^2$ and 10 $\mu\text{C/m}^2$, receptively, followed by the law of conservation of charge. From a view of a solid-solid interface for contact-separation mode with triboelectrification and electrostatic induction, the proposed TENG is approximated to a typically parallel-plate capacitor, so the potential distribution across the dielectric (air) is governed by the dielectric thickness or the distance between two triboelectric layers (PVDF and conductive fabrics), under a constant charge density. To reveal how the mechanical deformation/displacement (e.g., contact, separation, maximum-displacement, and approaching) impacts the triboelectric output, 2D cross-sectional geometries are introduced and analyzed electrically under various scenarios. The ground is connected to the outer edge of the surrounding air, and the free potential is selected at the conductive fabrics (electrodes) surface.

4.5. Data collection and ml models

The generated charge, current, and voltage signals from the MHAR-TENG were acquired by an electrometer (6514, Keithley) in a real-time manner, respectively. The whole dataset with a total number of 480000 samples built from 8 different users was used, and we divided it into 4 groups of data to perform the machine learning (i.e., 120,000 samples for each group data, 3 groups of data for training, and 1 for prediction). Then, a whole dataset was built from 8 different users, with a total number of 480000 samples, in which 75 % of data was used for training and 25 % for prediction. Concerning the individual voice recognition, 60,000 samples in charge, current, and voltage channels (marked as one group) were collected separately for each user when speaking a sentence “OPEN THE DOOR PLEASE.” The data training models used in the system were configured as follows: the principal component analysis (PCA) was used to implement the features for training, the Ensemble classifier (Bagged Trees) was used for data classification, and the confusion chart was obtained after training. Moreover, the prediction data processed with voice trained model was used for accuracy calculation and plotting confusion map. The training procedure for conventional TENG voice recognition remains consistent with the MHAR-TENG. Moreover, for the mode recognition, 60,000 samples in charge, current and voltage channels (marked as one group) were collected separately for one user when speaking a sentence “I FEEL SAD” in angry, happy, and sad modes. 4 group data in total were collected, 3 group data for training, and 1 for prediction. The flow chart and classifier remained consistent with the afore-mentioned voice recognition. The prediction data analyzed with mode trained model was used for accuracy calculation and plotting confusion map. The prediction accuracy was generally used to evaluate the model training results. The training models were developed in MATLAB and Python.

CRediT authorship contribution statement

Guojian Zhu: Writing **Yi Zhou**: Writing **Zeyu Si**: Funding acquisition **Yin Cheng**: Supervision **Fei Wu**: Methodology **Huan Wang**: Resources **Yaozong Pan**: Project administration **Jing Xie**: Data Curation **Chaobo Li**: Software **Aiying Chen**: Conceptualization **Ranran Wang**: Supervision **Jing Sun**: Resources.

Declaration of Competing Interest

The authors declare that they have no known competing financial interests or personal relationships that could have appeared to influence the work reported in this paper.

Data availability

The authors declare that the data supporting the findings of this study are available within the paper and its Supplementary Information files. All other data are available from the authors upon reasonable request.

Acknowledgments

Guojian Zhu and Yi Zhou contributed equally to this work. This work received the financial support from the following grants: National Natural Science Foundation of China (52203365, 61871368 and 62122080); the Austrian Chinese Cooperative Research and Development projects (GJHZ2046 and POWERTEX); Natural Science Foundation of Shanghai (22ZR1481700); Shanghai Pujiang Program (21PJ1414800).

Appendix A. Supporting information

Supplementary data associated with this article can be found in the online version at doi:10.1016/j.nanoen.2023.108237.

References

[1] J. Gubbi, R. Buyya, S. Marusic, M. Palaniswami, Internet of Things (IoT): a vision, architectural elements, and future directions, Future Gener. Comp. Syst. 29 (2013) 1645–1660.

[2] W.J.G. Ferguson, Y. Kuang, K.E. Evans, C.W. Smith, M. Zhu, Auxetic structure for increased power output of strain vibration energy harvester, Sens. Actuators, A 282 (2018) 90–96.

[3] J. Yang, et al., Triboelectrification-based organic film nanogenerator for acoustic energy harvesting and self-powered active acoustic sensing, ACS Nano 8 (2014) 2649–2657.

[4] J.H. Han, et al., Machine learning-based self-powered acoustic sensor for speaker recognition, Nano Energy 53 (2018) 658–665.

[5] W. Dong, et al., Soft human-machine interfaces: design, sensing and stimulation, Int. J. Intell. Robot. 2 (2018) 313–338.

[6] Y. Liu, et al., Epidermal mechano-acoustic sensing electronics for cardiovascular diagnostics and human-machine interfaces, Sci. Adv. 2 (2016), e1601185.

[7] J. Yang, et al., Eardrum-inspired active sensors for self-powered cardiovascular system characterization and throat-attached anti-interference voice recognition, Adv. Mater. 27 (2015) 1316.

[8] J.A. Paradiso, T. Starner, Energy scavenging for mobile and wireless electronics, IEEE Pervas. Comput. 4 (2005) 18–27.

[9] B. Li, J.H. You, Y.-J. Kim, Low frequency acoustic energy harvesting using PZT piezoelectric plates in a straight tube resonator, Smart Mater. Struct. 22 (2013), 055013.

[10] Izhar, F.U. Khan, Three degree of freedom acoustic energy harvester using improved Helmholtz resonator, Int. J. Precis. Eng. Man. 19 (2018) 143–154.

[11] K.H. Sun, J.E. Kim, J. Kim, K. Song, Sound energy harvesting using a doubly coiled-up acoustic metamaterial cavity, Smart Mater. Struct. 26 (2017), 075011.

[12] M. Yuan, H. Ji, J. Qiu, T. Ma, Active control of sound transmission through a stiffened panel using a hybrid control strategy, J. Intell. Mater. Syst. Struct. 23 (2012) 791–803.

[13] M. Yuan, Z. Cao, J. Luo, Z. Pang, Low frequency acoustic energy harvester based on a planar Helmholtz resonator, AIP Adv. 8 (2018), 085012.

[14] F.-R. Fan, Z.-Q. Tian, Z.L. Wang, Flexible triboelectric generator!, Nano Energy 1 (2012) 328–334.

[15] H. Guo, et al., Freestanding triboelectric nanogenerator enables noncontact motion-tracking and positioning, ACS Nano 12 (2018) 3461–3467.

[16] X. Cao, et al., Inductor-free wireless energy delivery via maxwell's displacement current from an electrodeless triboelectric nanogenerator, Adv. Mater. 30 (2018) 1704077.

[17] J. Liu, et al., A three-dimensional integrated nanogenerator for effectively harvesting sound energy from the environment, Nanoscale 8 (2016) 4938–4944.

[18] W. Qiu, Y. Feng, N. Luo, S. Chen, D. Wang, Sandwich-like sound-driven triboelectric nanogenerator for energy harvesting and electrochromic based on Cu foam, Nano Energy 70 (2020), 104543.

[19] H. Zhao, et al., Dual-tube Helmholtz resonator-based triboelectric nanogenerator for highly efficient harvesting of acoustic energy, Adv. Energy Mater. 9 (2019) 1902824.

[20] M. Yuan, C. Li, H. Liu, Q. Xu, Y. Xie, A 3D-printed acoustic triboelectric nanogenerator for quarter-wavelength acoustic energy harvesting and self-powered edge sensing, Nano Energy 85 (2021), 105962.

[21] Q. Zhang, et al., Multi-tube Helmholtz resonator based triboelectric nanogenerator for broadband acoustic energy harvesting, Front. Mater. 9 (2022), 896953.

[22] H. Yuan, et al., A high-performance coniform helmholtz resonator-basedtriboelectric nanogenerator for acoustic energy harvesting, Nanomaterials 11 (2021) 3431.

[23] C. Lang, J. Fang, H. Shao, X. Ding, T. Lin, High-sensitivity acoustic sensors from nanofibre webs, Nat. Commun. 7 (2016), 11108.

[24] W. Li, et al., Sensitivity-enhanced wearable active voiceprint sensor based on cellular polypropylene piezoelectret, ACS Appl. Mater. Interfaces 9 (2017) 23716–23722.

[25] W. Li, et al., Nanogenerator-based dual-functional and self-powered thin patch loudspeaker or microphone for flexible electronics, Nat. Commun. 8 (2017), 15310.

[26] K.Y. Lee, et al., Controllable charge transfer by ferroelectric polarization mediated triboelectricity, Adv. Funct. Mater. 26 (2016) 3067–3073.

[27] F. Liu, et al., Acoustic energy harvesting using an electromechanical Helmholtz resonator, J. Acoust. Soc. Am. 123 (2008) 1983–1990.

[28] M. Yuan, X. Sheng, Z. Cao, Z. Pang, G. Huang, Joint acoustic energy harvesting and noise suppression using deep-subwavelength acoustic device, Smart Mater. Struct. 29 (2020), 035012.

[29] Z.L. Wang, A.C. Wang, On the origin of contact-electrification, Mater. Today 30 (2019) 34–51.

[30] M.A. Pillai, E. Deenadayalan, A review of acoustic energy harvesting, Int. J. Precis. Eng. Manuf. 15 (2014) 949–965.

[31] J. Carbajo, J. Ramis, L. Godinho, P. Amado-Mendes, J. Alba, A finite element model of perforated panel absorbers including viscothermal effects, Appl. Acoust. 90 (2015) 1–8.

[32] Y. Wang, et al., A renewable low-frequency acoustic energy harvesting noise barrier for high-speed railways using a Helmholtz resonator and a PVDF film, Appl. Energy 230 (2018) 52–61.

[33] S. Niu, Z.L. Wang, Theoretical systems of triboelectric nanogenerators, Nano Energy 14 (2015) 161–192.

[34] J. Zhao, et al., Remarkable merits of triboelectric nanogenerator than electromagnetic generator for harvesting small-amplitude mechanical energy, Nano Energy 61 (2019) 111–118.

[35] F. Chen, et al., A novel triboelectric nanogenerator based on electrospun polyvinylidene fluoride nanofibers for effective acoustic energy harvesting and self-powered multifunctional sensing, Nano Energy 56 (2019) 241–251.

[36] Z. Wang, et al., A universal power management strategy based on novel sound-driven triboelectric nanogenerator and its fully self-powered wireless system applications, Adv. Funct. Mater. 31 (2021), 2103081.

[37] N. Cui, et al., High performance sound driven triboelectric nanogenerator for harvesting noise energy, Nano Energy 15 (2015) 321–328.

[38] C. Lang, et al., High-output acoustoelectric power generators from poly (vinylidenefluoride-co-trifluoroethylene) electrospun nano-nonwovens, Nano Energy 35 (2017) 146–153.

[39] J. Zheng, et al., Acoustic core-shell resonance harvester for application of artificial cochlea based on the piezo-triboelectric effect, ACS Nano 15 (2021) 17499–17507.

[40] Z. Yu, et al., Nanoporous PVDF hollow fiber employed piezo-tribo nanogenerator for effective acoustic harvesting, ACS Appl. Mater. Interfaces 13 (2021) 26981–26988.

[41] X. Fan, et al., Ultrathin, rollable, paper-based triboelectric nanogenerator for acoustic energy harvesting and self-powered sound recording, ACS Nano 9 (2015) 4236–4243.

[42] H. Shao, et al., Efficient conversion of sound noise into electric energy using electrospun polyacrylonitrile membranes, Nano Energy 75 (2020), 104956.

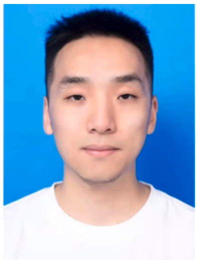

Zhu Guojian received his BS degree in material science and engineering from Henan University of Technology and now is a Joint-supervision candidate in SICCAS in Prof. Sun Jing's group. His research interest is acoustic energy harvester based on Triboelectric nanogenerator.

Zhou Yi received his B.Eng. degree (2017) in Nuclear Engineering and Technology from Lanzhou University and M.Sc. degree (2019) in Physics from Harbin Institute of Technology. He is now a Ph.D. candidate at Electrical and Computer Engineering, National University of Singapore. His research interests include photothermal management and energy harvesting, radioisotope power systems (RPS), hybrid energy systems, novel power technology and conversion.

Si Zeyu received the B.S.degree(2016) in marine technology from Ocean University of China.He is now working as an engineer of acoustic transducer and acoustic detection in Qingdao Branch, Institute of Acoustics, Chinese Academy of Sciences.

Cheng Yin received the B.S. degree (2011) in materials science and engineering from North China Electric Power University (Beijing) and the Ph.D. degree (2016) in Materials Physics and Chemistry from Shanghai Institute of Ceramics, Chinese Academy of Sciences (SICCAS). He is now working as an associate Professor in SICCAS, focusing on flexible and wearable electronics.

Wu Fei received her B.S. degree (2020) in materials science and engineering from Qingdao University of Technology and now is a MA. Eng candidate in Shanghai Institute of Ceramics, Chinese Academy of Sciences (SICCAS) in Prof. Sun Jing's group. Her research interest is multifunctional fiber sensors for wearable electronics.

Wang Huan received the BS degree in communication engineering (2011) and the MS degree in communication and information systems (2014) from Beijing University of Posts and Telecommunications. She is now working as an assistant researcher in the Institute of Microelectronics, Chinese Academy of Sciences, focusing on micro nano manufacturing technology research.

Pan Yaozong received his B.S. degree (2005) from Ocean University of China and Ph.D. degree (2010) from University of Chinese Academy of Sciences. He is now working as a Professor in Qingdao Branch of Institute of Acoustics. His research interest is acoustic transducer.

Xie Jing received the B.S. degree (2006) in Department of Electronics from Tsinghua University and the Ph.D. degree (2011) in microelectronics and solid-state electronics from the Institute of Semiconductors of the Chinese Academy of Sciences. She is now working as an Associate Researcher in the Institute of Microelectronics of the Chinese Academy of Sciences, focusing on MEMS technology and equipment system.

Li Chaobo received his B.S. degree (2001) from Shandong University and Ph.D. degree (2007) from Institute of Microelectronics. He is now working as a Professor in Institute of Microelectronics. His research interests include new principle of nanofabrication process and equipment, intelligent equipment.

Chen Aiying received her Ph.D. degree (2008) from Shanghai Jiao Tong University. She is now working as a Professor in University of Shanghai for Science and Technology. Her research interests include surface functionalization of nano porous materials and new type of battery materials.

Wang Ranran received her B.S. degree (2007) from China University of Petroleum and Ph.D. degree (2012) from SICCAS. She is now working as a Professor in SICCAS. Her research interests include low dimensional conductive materials, stretchable electrodes and conductors, flexible and wearable sensors.

Sun Jing received her M.S. from Changchun Institute of Applied Chemistry and Ph.D. degree from Shanghai Institute of Ceramics in 1994 and 1997, respectively. Then she joined Shanghai Institute of Ceramics (SICCAS). She spent one year as visiting scientist in Institute for Surface Chemistry in Stockholm (YKI) between 1999 and 2000 and as a JSPS fellow in National Institute of Advanced Science and Technology (AIST) in Japan during 2002–2004. She has been appointed as a Professor in SICCAS since 2005 and now is leading a research group focusing on photo-catalysis for indoors & outdoors air-cleaning and flexible electronics.